Journal of Power Sources 238 (2013) 109–116

Contents lists available at SciVerse ScienceDirect

Journal of Power Sources

journal homepage: www.elsevier.com/locate/jpowsour

Stabilization of $Cu/ZnO/ZrO_2$ catalyst for methanol steam reforming to hydrogen by coprecipitation on zirconia support

Yasuyuki Matsumura*

National Institute of Advanced Industrial Science and Technology (AIST), Kansai Center, Midorigaoka, Ikeda, Osaka 563-8577, Japan

HIGHLIGHTS

- $Cu/ZnO/ZrO_2$ catalyst supported on a ZrO_2 has been prepared.
- Cu sintering in $Cu/ZnO/ZrO_2$ is suppressed in the presence of the ZrO_2 support.
- Cu dispersion is high in comparison with $Cu/ZnO/ZrO_2$ without the support.
- Despite low Cu content, the composite catalyst is active and durable.

GRAPHICAL ABSTRACT

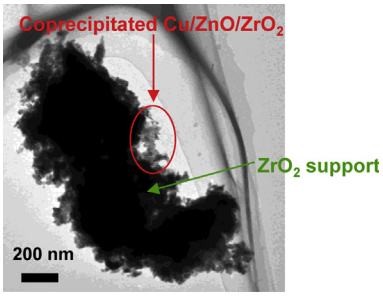

ARTICLE INFO

Article history:
Received 15 November 2012
Received in revised form
11 March 2013
Accepted 12 March 2013
Available online 26 March 2013

Keywords:
Coprecipitation
Support
Stabilization
Methanol steam reforming
$Cu/ZnO/ZrO_2$
Hydrogen production

ABSTRACT

Catalytic activity of $Cu/ZnO/ZrO_2$ for methanol steam reforming to hydrogen is stabilized by coprecipitation of $Cu/ZnO/ZrO_2$ on a zirconia support. The coprecipitate coarsely covers the surface of the support while the particle structure is similar to that without the support. Deactivation of $Cu/ZnO/ZrO_2$ in methanol steam reforming at 400 or 500 °C is mitigated in the presence of the support which suppresses the sintering of Cu particles. Although the Cu content of a supported catalyst is a half of that without the support, the activity of the supported catalyst is appreciably higher after the reaction at 400 °C for 5 h due to the higher Cu dispersion and surface activity.

1. Introduction

Copper catalysts are widely used in chemical industries for hydrogenation and dehydrogenation of hydrocarbons, methanol synthesis, and hydrogen production. They are often prepared by a coprecipitation method because Cu particles can be dispersed with the other particles that are usually metal oxides as promoters and/or stabilizers [1]. For example, $Cu/ZnO/Al_2O_3$ is a typical coprecipitated catalyst for methanol synthesis and methanol steam reforming [1–3]. The catalyst is active and selective, but it is deactivated at above 300 °C mainly due to the sintering of Cu particles [2,3]. The catalyst is not suitable for compact hydrogen processors from methanol to feed hydrogen to polymer electrolyte fuel cells (PEFCs) utilized in electric vehicles, because the reaction temperature often fluctuates and exceeds 300 °C under DSS (daily start and stop) operation mode [4,5]. Hence, stable catalysts are required for this application. Alloy catalysts such as Pd–Zn are known to be active to methanol steam reforming and rather stable at high temperatures [2], but the high cost of palladium is an indispensable problem.

* Tel.: +81 72 751 7821; fax: +81 72 751 9623.
E-mail address: yasu-matsumura@aist.go.jp.

0378-7753/$ – see front matter © 2013 Elsevier B.V. All rights reserved.
http://dx.doi.org/10.1016/j.jpowsour.2013.03.074

It was previously reported that coprecipitated $Cu/ZnO/ZrO_2$ is fairly durable in the methanol steam reforming ($CH_3OH + H_2O \rightarrow 3H_2 + CO_2$) at 400 °C, but the sintering of copper proceeds under the reductive condition [6,7]. Under the same conditions, a commercial $Cu/ZnO/Al_2O_3$ was steeply deactivated [6] while the activity of $Cu/ZnO/ZrO_2$ below 300 °C is comparable to that of $Cu/ZnO/Al_2O_3$ [7–10]. Addition of ZrO_2 to Cu/ZnO in the coprecipitation process results in high dispersion of Cu and ZnO particles and the sintering is suppressed by virtue of the presence of amorphous ZrO_2 particles in the coprecipitate, while the ZrO_2 particles do not directly affect the surface activity of copper [7]. Jones and Hagelin-Weaver prepared $Cu/ZnO/ZrO_2$ supported on Al_2O_3 and/or ZrO_2 nanoparticles by the impregnation method [11]. The activity of the supported catalyst to methanol steam reforming was often comparable with a coprecipitated $Cu/ZnO/Al_2O_3$ despite the lower Cu surface area. This suggests that the usage of the support material may enhance the catalytic activity of Cu surface. It is known that formation of metal hydroxides proceeds selectively on the surface of oxide supports in an aqueous solution of the metal ions with an increase in the pH [12,13]. The deposition-precipitation process may be applied to the coprecipitation on the support surface and increase the Cu dispersion. Hence, the coprecipitation of $Cu/ZnO/ZrO_2$ has been attempted on a ZrO_2 support with high surface area. In the present study, it will be shown that $Cu/ZnO/ZrO_2$ is successfully coprecipitated on the ZrO_2 support and the catalyst with the unique structure is active and stable in the methanol steam reforming at 400 °C or above in comparison with a simple coprecipitated catalyst.

2. Experimental

A $Cu/ZnO/ZrO_2$ catalyst was prepared by coprecipitation from a 0.5-M aqueous mixture of $Cu(NO_3)_2 \cdot 3H_2O$ (Wako Pure Chemical, S grade), $Zn(NO_3)_2 \cdot 6H_2O$ (Wako, S), and $ZrO(NO_3)_2 \cdot 2H_2O$ (Wako, 1st) with addition of an aqueous solution of Na_2CO_3 (0.5 M) under vigorous stirring at 80 °C as described elsewhere [6]. The atomic ratio of Cu/Zn/Zr was 1.0/1.0/0.5. After filtration and washing with distilled water, the precipitate was dried at 120 °C for 15 h and finally calcined in air at 500 °C for 12 h. The Cu content of this catalyst denoted as CZZ was 30 wt.% in the reduced form. Supported catalysts were prepared by the deposition of $Cu/ZnO/ZrO_2$ on a ZrO_2 support supplied from Catalysis Society of Japan (reference catalyst, JRC–ZRO–2; the specific surface area is 254 $m^2\ g^{-1}$ and the ignition loss is 12.73%). The ZrO_2 powder was suspended in the starting solution of CZZ by vigorous stirring at 80 °C and the Na_2CO_3 solution was added. There were no significant differences in the procedure from the usual coprecipitation method except for the existence of the support. The resulting catalysts containing 50 and 30 wt.% of the coprecipitate (as reduced form) were designated as $50CZZ/ZrO_2$ (Cu content, 15 wt.%) and $30CZZ/ZrO_2$ (9 wt.%), respectively. The catalysts were also dried at 120 °C for 15 h and finally calcined in air at 500 °C for 12 h.

Catalytic tests were performed in a fixed-bed continuous-flow reactor operated under atmospheric pressure. Zirconia balls (1 mm in diameter) were mixed with a powder catalyst (50–100 mesh) whose weight (W) was 0.10–0.50 g, in order to reduce back pressure during the reaction and keep sufficient length of the catalyst layer (2.0 g in total of the catalyst and the balls). The mixture was placed in a tubular reactor made of stainless steel (i.d., 7 mm) with quartz-wool plugs. The catalyst was pre-reduced with a reaction mixture of methanol, steam, and argon (1.0/1.2/0.5 in molar ratio) with a flow rate (F) of 27 $dm^3\ h^{-1}$ at 250 °C for 1 h; then the reactor was heated up to 400 °C in the reaction flow. The effluent gas was dried with a cold trap at ca. −50 °C, and analyzed with an on-stream gas chromatograph (Shimadzu GC-8A; activated carbon, 2 m; Ar carrier) equipped with a thermal conductivity detector (TCD). After the reaction for 8 h, the catalyst was cooled to room temperature under an Ar stream for 12 h or longer.

The methanol conversion was determined from the material balance of the reactant and the products. The error was within 5%. No formation of formaldehyde or methyl formate was observed. The selectivities of CO and CH_4 were calculated in molar basis [14].

The structures of the catalysts were evaluated by transmission electron microscopy (TEM) and high-angle annular dark field imaging in scanning TEM (HAADF/STEM) with energy dispersed X-ray spectroscopic (EDS) analysis using an FEI Tecnai G^2 F20 Twin at an acceleration voltage of 120 kV.

Powder X-ray diffraction (XRD) patterns of the catalysts were recorded in air at room temperature with an MAC Science MP6XCE diffractometer using nickel-filtered Cu Kα radiation. Mean crystallite sizes of the particles detected by XRD were determined from the line broadening of the attributed peaks using Scherrer equation [15].

The specific surface areas of the catalysts were determined from the isotherms of nitrogen physisorption using the method of Brunauer, Emmet, and Teller (BET).

X-ray photoelectron spectra (XPS) were recorded at room temperature with a JEOL JPS-9010MX spectrometer (Al Kα). The catalyst taken out from the reactor was mounted to a sample holder with a carbon tape in air. Since the sample was gradually oxidized in air, Ar sputtering (400 V, 7 mA) was carried out for 5 s to remove oxygen adsorbed on the surface. No sputtering was carried out with the catalysts as prepared. Binding energies were corrected by the reference of the C 1s line at 284.6 eV. The surface atomic concentrations of Cu, Zn, Zr, and O were calculated from the peak areas using the average matrix relative sensitivity factors (AMRSFs) of Cu $2p_{3/2}$ (32), Zn $2p_{3/2}$ (39), Zr 3d (5.5), and O 1s (3.4) [16]. The contribution of carbon from the tape and contaminates to the concentrations was ignored. Since the peak intensity relates to the electron inelastic mean free path of electron for the surface substance, the surface concentrations were corrected using the values of 2.1 nm (Cu), 2.5 nm (CuO), and 2.7 nm (ZnO and ZrO_2) [16]. The AMRSFs were determined by measuring standard materials of Cu, Zn, and Zr metal plates and an alumina plate. The uncertainty of AMRSFs is less than 2% [16].

On the basis of the stoichiometry, $N_2O + 2Cu \rightarrow N_2 + Cu_2O$, the surface Cu amount of the catalyst was determined using a BELCAT (BEL Japan) reaction system [17]. The surface of the sample reduced with hydrogen at 250 °C for 1 h was oxidized by the decomposition of N_2O at 50 °C. After the reduction, the sample (0.5 g) was cooled to 50 °C in a flow of helium and pulses of N_2O were fed. Nitrogen produced was separated with a gas chromatograph and the amount of N_2 was measured with a TCD.

3. Results and discussion

3.1. Structure of $Cu/ZnO/ZrO_2$ coprecipitated on ZrO_2 support

The TEM image of $30CZZ/ZrO_2$ after the calcination at 500 °C shows that small particles are deposited on the grains of the ZrO_2 support (Fig. 1). In order to confirm the structure, EDS analysis was carried out in the part surrounded by a square in Fig. 1. No obvious presence of Zr is detected on the points 1 and 2 in the aggregate of small particles (Fig. 2), but Zr is mainly present on the points 3–5 which are probably located on the ZrO_2 support. Hence, the ZrO_2 support is manly present at the black portion in Fig. 1 and the gray portions around the black body are the images of the coprecipitated particles. Coexistence of Cu and/or Zn on the points 3–5 suggests that the surface of the support is covered with the coprecipitated particles. The TEM image of $50CZZ/ZrO_2$ is similar to that in Fig. 1, but the part of small particles deposited on the surface is larger (not

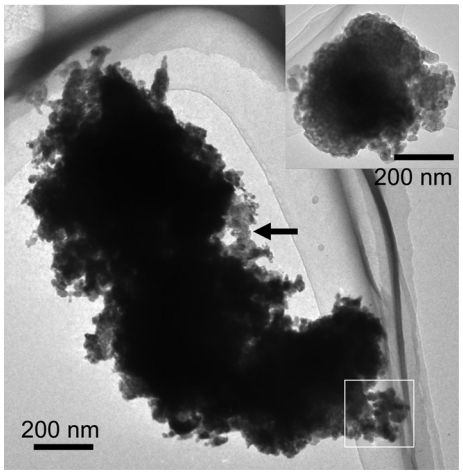

Fig. 1. TEM image of 30CZZ/ZrO_2 as prepared. Inset, ZrO_2 support after calcination at 500 °C for 12 h. Gray portions such as a part indicated by an arrow are the images of the coprecipitated particles.

shown). The size of the aggregate for 30 or 50CZZ/ZrO_2 is usually larger than that of the ZrO_2 support shown in the inset of Fig. 1, probably because ZrO_2 support grains covered with the coprecipitate gather and form a large grain.

The XRD pattern of the aurichalcite $(Cu,Zn)_5(CO_3)_2(OH)_6$ phase is mostly recorded with CZZ just after the coprecipitation followed by drying at 120 °C as reported by Matter et al. (Fig. 3a) [18,19]. The peaks for aurichalcite are also present in the patterns for 50 and 30CZZ/ZrO_2 (Fig. 3b and c). The XRD pattern of the ZrO_2 support shows that the zirconia is amorphous (Fig. 3d). The high ignition loss of the support material suggests presence of a significant amount of hydroxyl groups on the surface, and it may increase the affinity with the coprecipitate as can be seen in Fig. 1. The mean crystallite size of aurichalcite in CZZ is determined as 14 nm from

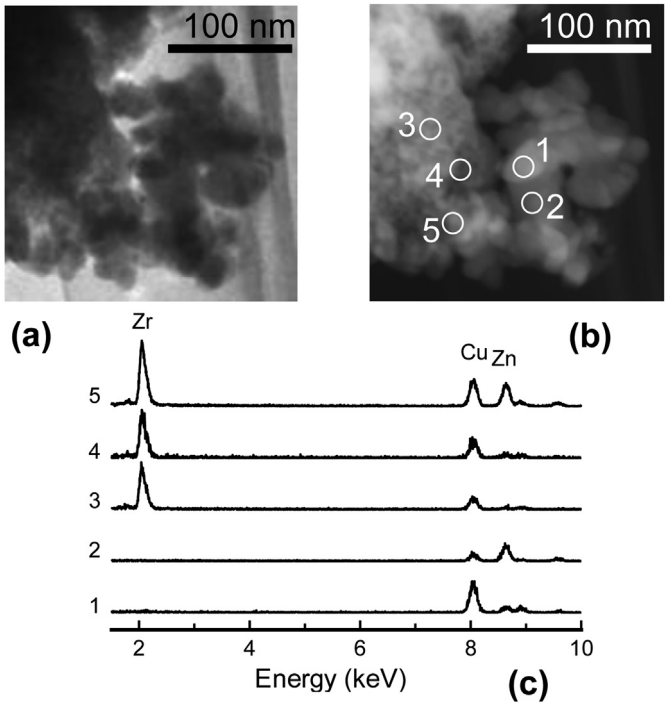

Fig. 2. TEM and HAADF/STEM images and EDS analysis of 30CZZ/ZrO_2. (a) TEM image, (b) HAADF/STEM image, and (c) EDS spectra on points 1–5.

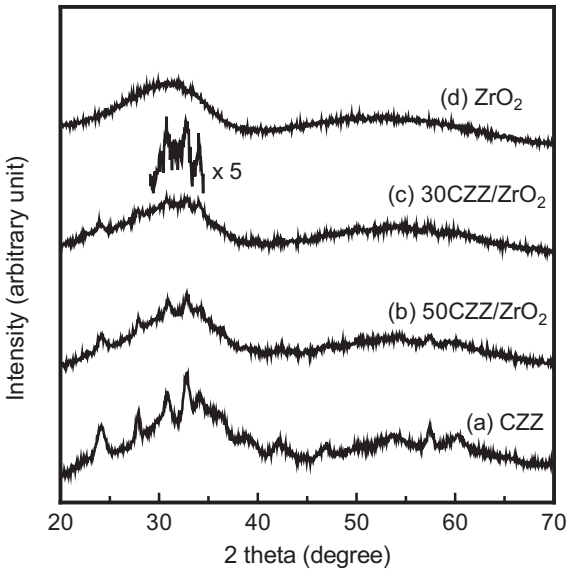

Fig. 3. XRD patterns of the precipitates after drying at 120 °C. (a) CZZ, (b) 50CZZ/ZrO_2, (c) 30CZZ/ZrO_2, and (d) ZrO_2 support as received.

the line broadening of the peak at 32.8° in 2θ. The sizes for 50 and 30CZZ/ZrO_2 are 16 and 14 nm, respectively, showing that the coprecipitate on the support is similar to that without the support. After the calcination in air at 500 °C, there are XRD peaks attributed to CuO and ZnO in the pattern of CZZ (Fig. 4a) [18]. A broad and small peak at 30.5° can be attributed to tetragonal ZrO_2 [18]. Since the peak intensity is weak, the major part of ZrO_2 is probably still amorphous [6,7]. The peaks attributed to tetragonal ZrO_2 are significant in the patterns for 50 and 30CZZ/ZrO_2 with the peaks for CuO and ZnO (Fig. 4b and c) [18]. Interestingly the XRD pattern of the ZrO_2 support after the calcination at 500 °C for 12 h is mostly that of the monoclinic phase (Fig. 4d) [18], showing the phase transition from amorphous to monoclinic during the calcination. The mean crystallite size of the monoclinic ZrO_2 is determined as 14 nm from the line broadening of the peak at 28.3°. The absence of monoclinic ZrO_2 in 50 and 30CZZ/ZrO_2 suggests that the presence

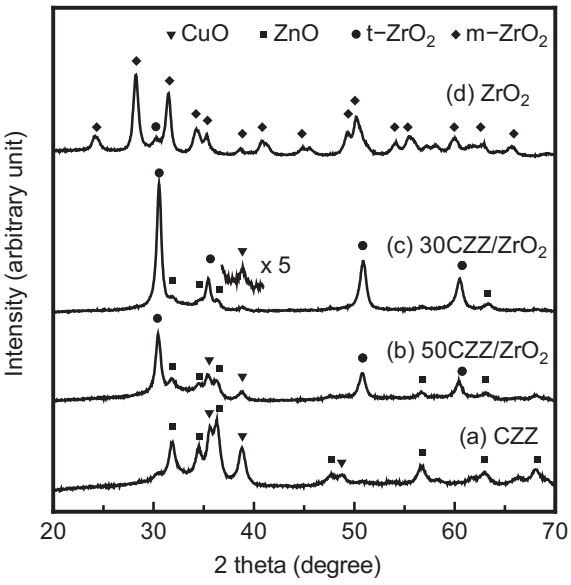

Fig. 4. XRD patterns of Cu catalysts as prepared. (a) CZZ, (b) 50CZZ/ZrO_2, (c) 30CZZ/ZrO_2, and (d) ZrO_2 support heated in air at 500 °C for 12 h.

Table 1
Mean crystallite sizes of the Cu catalysts.

Catalyst	Main reaction temperature (°C)	Mean crystallite size (nm)		
		Cu (CuO)[a]	ZnO	ZrO_2
CZZ	As prepared	(12)	11	7
50CZZ/ZrO_2	As prepared	(12)	9	13
30CZZ/ZrO_2	As prepared	(13)	10	15
CZZ	400	14	13	10
CZZ	500	17	13	13
50CZZ/ZrO_2	400	12	12	14
50CZZ/ZrO_2	500	14	15	16
30CZZ/ZrO_2	400	12	14	14
30CZZ/ZrO_2	500	12	14	15

[a] In parenthesis the size for CuO is given.

of the coprecipitate on the support surface promotes the phase transition of the support to tetragonal ZrO_2. Murase et al. reported the phase transition of monoclinic ZrO_2 to tetragonal phase at 300 °C in the presence of metal oxides such as MgO on the surface possibly because of change in the surface energy by the interaction with the metal oxides [20]. The mean crystallite size of CuO is calculated from the line broadening at 38.8°, assuming overlapping of two equivalent peaks [CuO(−1 1 1) and CuO(1 1 1)] with the separation of 0.21° [18]. The size is 12–13 nm regardless of the samples (Table 1). The size for ZnO is determined from the broadening at 31.7°. These sizes for 50 and 30CZZ/ZrO_2 are similar to those for CZZ (see Table 1).

The BET surface area for CZZ as prepared is 48 $m^2 g^{-1}$ (Table 2). The area for 50CZZ/ZrO_2 is 57 $m^2 g^{-1}$, appreciably higher than that for CZZ, while the area for 30CZZ/ZrO_2 is 52 $m^2 g^{-1}$. The BET surface area of the ZrO_2 support calcined at 500 °C is as small as 39 $m^2 g^{-1}$. This suggests that the surface area of the support does not cause the higher surface areas of 50 and 30CZZ/ZrO_2 and the area of the coprecipitate on the support contributes significantly to the surface area.

The surface of the catalyst after the calcination at 500 °C was analyzed by XPS (see Table 2). The binding energies of Cu $2p_{3/2}$, Zn $2p_{3/2}$, and Zr $3d_{5/2}$ are 933.5–933.7, 1021.9, and 181.9–182.0 eV, respectively, regardless of the samples [21]. The surface atomic concentrations of Cu^{2+} and Zn^{2+} decline with a decrease in the amount of surface coprecipitate. On the other hand, the concentration of Zr^{4+} increases probably because the surface of the ZrO_2 support is partly exposed. The surface concentration of Zr^{4+} for the ZrO_2 support calcined at 500 °C is 43%. The Zr^{4+} concentrations for 50 and 30CZZ/ZrO_2 are significantly smaller than that for the support, while the surface deposit also contains zirconium ions. Assuming that the intensity of the Zr 3d lines from the coprecipitate relates to the intensity of the Zn $2p_{3/2}$ line, the surface concentrations of Zr^{4+} contributed from the coprecipitate are calculated as 11% for 50CZZ/ZrO_2 and 7% for 30CZZ/ZrO_2 from the atomic ratio of Zr^{4+}/Zn^{2+} for

Table 2
Specific surface area and surface atomic concentrations of the Cu catalysts.

Catalyst	Main reaction temperature (°C)	BET surface area ($m^2 g^{-1}$)	Surface atomic concentration (%)		
			Cu (Cu^{2+})[a]	Zn^{2+}	Zr^{4+}
ZrO_2	Calcined at 500 °C	39	–	–	43
CZZ	As prepared	48	(7.5)	13	16
50CZZ/ZrO_2	As prepared	57	(5.5)	9.2	20
30CZZ/ZrO_2	As prepared	52	(4.6)	5.9	25
CZZ	400	43	8.8	14	17
CZZ	500	37	6.7	13	18
50CZZ/ZrO_2	400	47	5.4	9.6	23
50CZZ/ZrO_2	500	32	5.6	8.8	27
30CZZ/ZrO_2	400	43	3.8	5.8	30
30CZZ/ZrO_2	500	39	3.8	5.4	34

[a] In parenthesis the atomic concentration of Cu^{2+} is given.

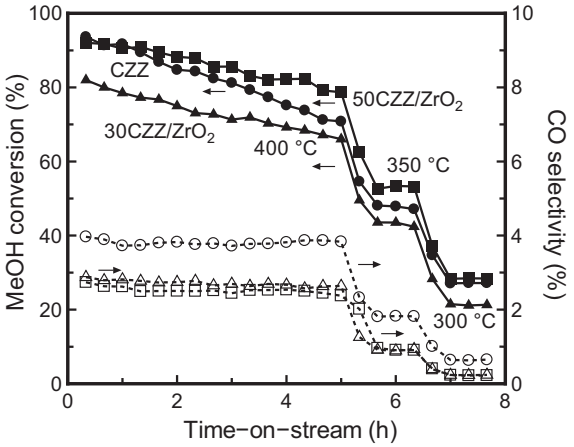

Fig. 5. Activity of Cu catalysts in methanol steam reforming mainly at 400 °C with *W*/*F* of 0.0055 g h dm^{-3}. Circle symbols, CZZ; square, 50CZZ/ZrO_2; triangle, 30CZZ/ZrO_2.

CZZ. That is, the Zr^{4+} concentrations from the ZrO_2 support are approximately estimated as 9% for 50CZZ/ZrO_2 and 18% for 30CZZ/ZrO_2. Hence, it is suggested that a half of the support surface in 30CZZ/ZrO_2 is not covered with the coprecipitate and the coverage for 50CZZ/ZrO_2 is higher due to the thicker surface layer.

3.2. Steam reforming of methanol over the Cu catalysts

In order to evaluate the durability of the Cu catalysts at a high temperature, methanol steam reforming was carried out at 400 °C. Hydrogen and carbon dioxide are mainly produced over CZZ and no formation of methane is detected. The activity of CZZ decreases gradually with an increase in the time period of the reaction (Fig. 5; *W*/*F*, 0.0055 g h dm^{-3}) as reported previously [6,7]. After the reaction at 400 °C for 5 h, the activities at 350 and 300 °C were examined. While the Cu content of 50CZZ/ZrO_2 is a half of that for CZZ, the initial activity of 50CZZ/ZrO_2 at 400 °C is similar to that of the latter and the activity after the reaction for 5 h is significantly higher. The activity of 30CZZ/ZrO_2 is lower than that of CZZ. The by-production of carbon monoxide, which is unfavorable against PEFC, is significantly low with the support.

In order to accelerate the deactivation, the reaction was carried out at 500 °C for 5 h after the reaction at 400 °C for 1 h at the *W*/*F* of 0.0055 g h dm^{-3}; then, the activity at 400 °C was examined (Fig. 6). After the deactivation at 500 °C, the activity of 50CZZ/ZrO_2 at

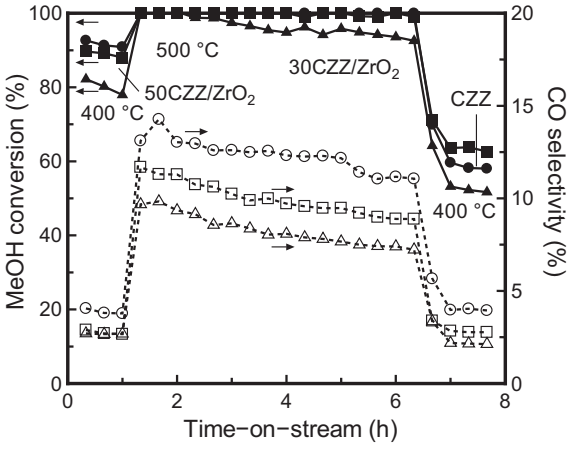

Fig. 6. Deactivation of Cu catalysts in methanol steam reforming mainly at 500 °C with *W*/*F* of 0.0055 g h dm^{-3}. Circle symbols, CZZ; square, 50CZZ/ZrO_2; triangle, 30CZZ/ZrO_2.

400 °C is discernibly higher than that of CZZ. In the reaction at 500 °C methane is slightly detected with the selectivity less than 0.1% regardless of the catalysts.

The reaction in Fig. 6 was also carried out at different *W*/*F*, and the dependence of the final activity at 400 °C on *W*/*F* is shown in Fig. 7. The by-production of carbon monoxide over $Cu/ZnO/Al_2O_3$ is mainly caused by the reverse water–gas shift reaction (RWGS, $CO_2 + H_2 \rightarrow CO + H_2O$) and the CO selectivity depends on the methanol conversion because carbon monoxide is a secondary product [22,23]. Also, the CO formation over $Cu/ZnO/ZrO_2$ is probably due to RWGS, at least in part, because the selectivity increases with an increase in the methanol conversion [6,7]. This suggests that the CO selectivity of the catalysts should be examined in consideration of the methanol conversion. In the case of 30CZZ/ZrO_2, the CO selectivity is 2.8% at the conversion of 66% at 400 °C and that with CZZ at the lower conversion of 58% is 4.0% (see Fig. 7). Thus, the CO by-production is also suppressed on 30CZZ/ZrO_2. The CO selectivity for 50CZZ/ZrO_2 is 2.8% at the conversion of 63% and the activity is higher than those for the other catalysts, showing that the optimum composite catalyst is 50CZZ/ZrO_2.

3.3. Sintering of Cu particles during reaction

Peaks for metallic Cu are recorded at 43.4° and 50.6° with the peaks attributed to ZnO in the XRD pattern of CZZ after the reaction mainly at 400 °C in Fig. 5 (Fig. 8a) [18]. A small peak attributed to tetragonal ZrO_2 is present at 30.4° while the major part of ZrO_2 is probably amorphous [6,7]. The mean crystallite sizes of Cu, ZnO, and ZrO_2 are calculated as 14, 13, and 10 nm, respectively (see Table 1). The size of Cu is determined from the broadening of the peak at 43.4°. After the reaction mainly at 500 °C in Fig. 6, the peaks for tetragonal ZrO_2 become significant (Fig. 8b), suggesting crystallization of amorphous ZrO_2 during the reaction. The peaks for Cu are intensified and the mean crystallite size of Cu increases to 17 nm, showing sintering of Cu particles. The presence of the amorphous ZrO_2 hinders the sintering of Cu particles as discussed in the previous works [6,7], but the crystallization of ZrO_2 probably weakens the hindrance effect. In the case of 50CZZ/ZrO_2 after the reaction mainly at 400 °C, the peaks for Cu, ZnO, and ZrO_2 are also present (Fig. 8c). The crystallite size of Cu is 12 nm and discernibly smaller than that of CZZ. The peaks are intensified after the reaction mainly at 500 °C (Fig. 8d). The Cu crystallite size is increased to 14 nm, while it is the same as that for CZZ after the reaction mainly at 400 °C. The peaks for Cu and ZnO are small in the XRD patterns for 30CZZ/ZrO_2 after the reactions (Fig. 8e and f). The crystallite size of Cu after the reaction mainly at 400 °C is 12 nm and the size is unchanged after the reaction mainly at 500 °C. This shows that the sintering of Cu particles is suppressed on the ZrO_2 support. Since the crystallite size of CuO for CZZ as prepared is similar to those for the other samples (see Table 1), the sintering of Cu particles proceeds considerably on CZZ even at 400 °C in comparison with the supported catalysts and it probably causes the steeper deactivation of CZZ in the reaction at 400 °C (see Fig. 5).

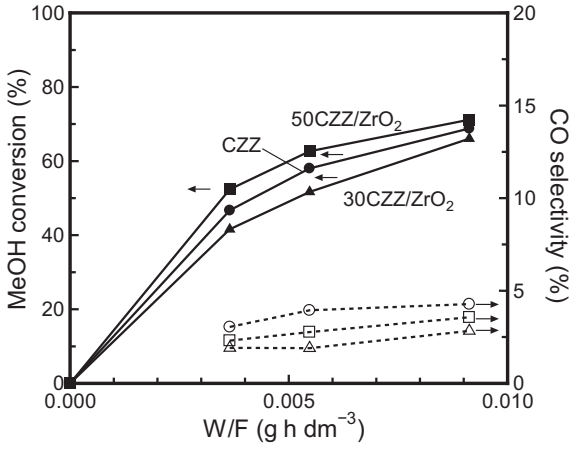

Fig. 7. Dependence of the activity of Cu catalysts at 400 °C on contact time (*W*/*F*) after the reaction at 500 °C. Circle symbols, CZZ; square, 50CZZ/ZrO_2; triangle, 30CZZ/ZrO_2.

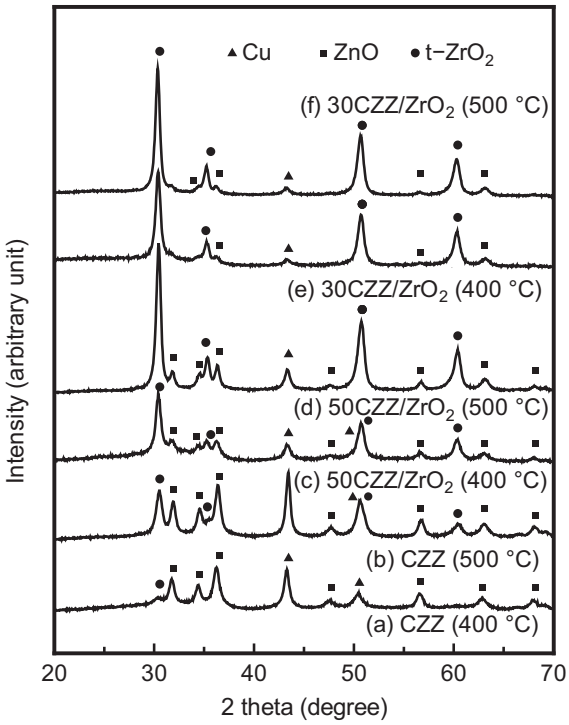

Fig. 8. XRD patterns of the catalysts after the reaction. (a) CZZ after the reaction mainly at 400 °C shown in Fig. 5, (b) CZZ after the reaction mainly at 500 °C shown in Fig. 6, (c) 50CZZ/ZrO_2 mainly at 400 °C, (d) 50CZZ/ZrO_2 mainly at 500 °C, (e) 30CZZ/ZrO_2 mainly at 400 °C, and (f) 30CZZ/ZrO_2 mainly at 500 °C.

3.4. Surface Cu amount of the catalysts after reaction

The BET surface area of CZZ after the reaction mainly at 400 °C in Fig. 5 is 43 $m^2\ g^{-1}$ and the area is decreased to 37 $m^2\ g^{-1}$ after the reaction mainly at 500 °C in Fig. 6 (see Table 2). The area for 50CZZ/ZrO_2 is considerably decreased to 32 $m^2\ g^{-1}$ after the reaction mainly at 500 °C, while the area is 47 $m^2\ g^{-1}$ after the reaction mainly at 400 °C. Since the intensity of the XRD peaks of ZrO_2 for the sample after the reaction mainly at 500 °C is significantly stronger than that after the reaction mainly at 400 °C (see Fig. 8), it is supposed that the decrease in the surface area at 500 °C is mainly caused by the structural change of the support. The change in the surface area for 30CZZ/ZrO_2 is fairly small, whereas the increase in the intensity of the XRD peaks for ZrO_2 is not large.

The surface atomic concentrations of the catalysts after the reactions in Figs. 5 and 6 were determined by XPS (see Table 2). The binding energies of Cu $2p_{3/2}$, Zn $2p_{3/2}$, and Zr $3d_{5/2}$ are 932.2–932.7, 1021.7–1022.0, and 182.2–182.6 eV, respectively, regardless of the samples. The energy of Cu $2p_{3/2}$ shows presence of metallic Cu on the surface after the Ar sputtering for 5 s [21]. The concentration of Cu is 9% for CZZ after the reaction mainly at 400 °C in Fig. 5 and it decreases to 7% after the reaction mainly at 500 °C in Fig. 6. On the other hand, the Cu concentrations for 50 and 30CZZ/ZrO_2 after the reaction mainly at 500 °C are each similar to those after 400 °C.

Table 3
Reaction parameters of the Cu catalysts.

Catalyst	Main reaction temperature (°C)	Cu surface amount[a] (mmol g^{-1})	Cu dispersion[b] (%)	MeOH consumption rate[c] (mmol s^{-1} g^{-1})	TOF at 400 °C[d] (s^{-1})
CZZ	400	1.4×10^{-1}	3	1.0	7.0
CZZ	500	9.2×10^{-2} (0.113)	2 (2.3)	0.55	6.0 (4.9)
50CZZ/ZrO_2	400	9.6×10^{-2}	4	1.5	1.6×10
50CZZ/ZrO_2	500	7.1×10^{-2} (0.087)	3 (3.7)	0.64	9.0 (7.2)
30CZZ/ZrO_2	400	6.4×10^{-2}	5	0.82	1.3×10
30CZZ/ZrO_2	500	5.9×10^{-2} (0.058)	4 (4.1)	0.47	7.9 (8.2)

[a] The amount was determined from the surface atomic concentration and BET surface area, while in parenthesis that from N_2O decomposition is given.
[b] In parenthesis Cu dispersion determined by N_2O decomposition is given.
[c] Methanol consumption rate at the methanol conversion of 50% in the reaction at 400 °C.
[d] In parenthesis TOF calculated from the Cu surface amount determined by N_2O decomposition is given.

The Cu surface amount can be estimated from the surface atomic concentrations and the BET surface area [6,7]. The Cu surface amount is calculated using the atomic site densities that are assumed as 0.032 mmol m^{-2} (Cu), 0.097 mmol m^{-2} (Zn^{2+}), 0.085 mmol m^{-2} (Zr^{4+}), and 0.030 mmol m^{-2} (O^{2-}) on the basis of the atomic/ionic radii. The Cu surface amount for CZZ is calculated as 0.1 mmol g^{-1} after the reaction mainly at 400 °C and it decreases discernibly after the reaction mainly at 500 °C (Table 3). The decrease in the Cu surface amount is also detected with 50CZZ/ZrO_2, but the decrease for 30CZZ/ZrO_2 is insignificant. The tendency is consistent with the change in the Cu crystallite size after the reaction at 500 °C (see Table 1), because the increase in the particle size results in decrease in the Cu surface amount.

In order to verify the Cu surface amount separately, the surface oxidation with N_2O was carried out with a different aliquot of the sample after the reaction mainly at 500 °C with the *W*/*F* of 0.018 g h dm^{-3} [17]. The surface Cu amounts for CZZ, 50CZZ/ZrO_2, and 30CZZ/ZrO_2 are determined as 0.113, 0.087, and 0.058 mmol g^{-1}, respectively. The values correspond fairly well with the amounts determined from the surface atomic concentrations (see Table 3). From these values the Cu surface amounts for 50 and 30CZZ/ZrO_2 are calculated as 77 and 51%, respectively, of that for CZZ. The Cu surface dispersion was obtained from the ratio of the Cu surface amount to the Cu content of the catalyst, and the values are 2.4% for CZZ, 3.7% for 50CZZ/ZrO_2, and 4.1% for 30CZZ/ZrO_2. If all the Cu particles are exposed and spherical with a diameter equal to the mean crystallite size, the dispersions for CZZ, 50CZZ/ZrO_2, and 30CZZ/ZrO_2 will be 6.1, 7.4, and 8.6%, respectively. Thus, 39% of Cu particle surface is assumed to be exposed in CZZ, while those for 50 and 30CZZ/ZrO_2 are 50 and 48%, respectively. Although the assumption is approximate, this simple calculation suggests that a significant part of the Cu surface is hidden in the aggregate of the coprecipitated particles [7] and the hidden portion is decreased by employing the support. However, the extent is not great and the smaller particle size in the supported catalyst also contributes to the higher dispersion.

3.5. Surface activity of the Cu catalysts

Turnover frequency (TOF) can be calculated from the methanol consumption rate and the Cu surface amount, but it varies with the methanol conversion which is not proportional to the contact time (*W*/*F*) (see Fig. 7) [23,24]. For example, the TOF of CZZ at the conversion of 47% in Fig. 7 is 5.1 s^{-1} (Cu surface amount, 0.113 mmol g^{-1}), but that at 69% is 3.0 s^{-1}. That is, the values of TOF should be compared at the same conversion. It was experimentally found that there is a linear fit between $1/(1 - C)$ and *W*/*F* (Fig. 9), where *C* is the methanol conversion below 80% [14]. The fit satisfies the reaction data for Cu/ZnO/Al_2O_3 reported by Purnama et al. [23]. On the basis of the relationship, the value of *W*/*F* producing a certain value of methanol conversion, e.g., 50%, can be estimated. Table 3 shows the methanol consumption rate at the conversion of 50% evaluated from the obtained value of *W*/*F*. The consumption rate should be a linear parameter of the catalytic activity.

The TOFs for 50 and 30CZZ/ZrO_2 after the reaction at 400 °C for 5 h are significantly higher than that for CZZ (see Table 3). Kniep et al. discussed that the structural disorder in Cu particle causes the high surface activity [25]. The sintering of the Cu particles during the reaction should cause the reduction of the disorder [6,7]. As discussed in the previous section, the sintering is rather promoted in CZZ even at 400 °C than in 50 or 30CZZ/ZrO_2. Hence, the lower TOF of CZZ may be due to the sintering during the reaction. After the reaction mainly at 500 °C, the TOF of 30CZZ/ZrO_2 also decreases in comparison with that after the reaction at 400 °C despite no significant change in the Cu crystallite size. Since high temperature enhances crystalline rearrangement, the disorder would decrease at 500 °C even when without the significant sintering. However, the mechanism of the decline in the surface activity is still unclear and the further investigation is required for the clarification.

It should be noted that the CO selectivity at 400 °C increases with an increase in the mean Cu crystallite size (Fig. 10). As described in the previous section, the selectivity depends on the methanol conversion; therefore, the values of the selectivity in the conversion range of 66–79% are plotted for comparison. Arena et al. reported that TOF for CO_2 hydrogenation at 200 °C over Cu/ZnO/ZrO_2 increases with an increase in the Cu particle size [26]. Hence, it

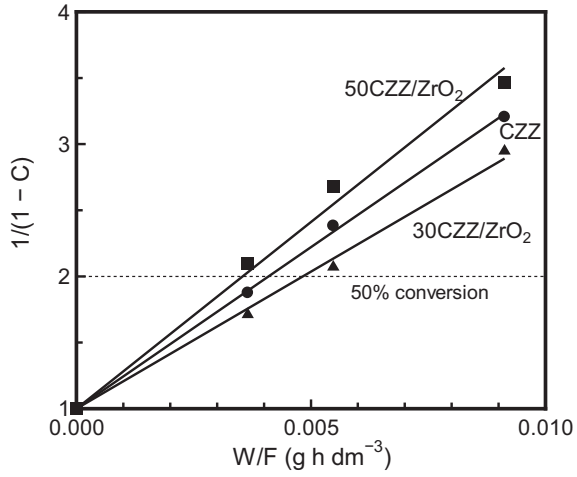

Fig. 9. Plots of $1/(1 - C)$ vs. *W*/*F* on the basis of the methanol conversions (*C*) for Cu catalysts shown in Fig. 7. Circle symbols, CZZ; square, 50CZZ/ZrO_2; triangle, 30CZZ/ZrO_2.

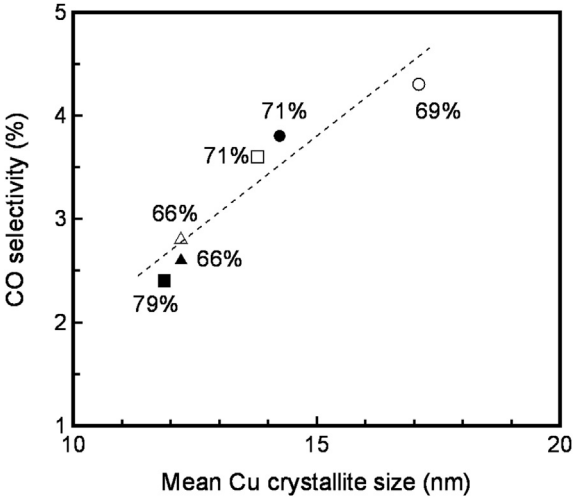

Fig. 10. Relationship between CO selectivity at 400 °C and mean Cu crystallite size in methanol conversion range of 66–79%. Circle symbols, CZZ; square, 50CZZ/ZrO_2; triangle, 30CZZ/ZrO_2. Solid symbols show the data in Fig. 5 at W/F of 0.0055 g h dm^{-3} and open symbols show the data in Fig. 7 at W/F of 0.0091 g h dm^{-3}. In the figure, the methanol conversions are given.

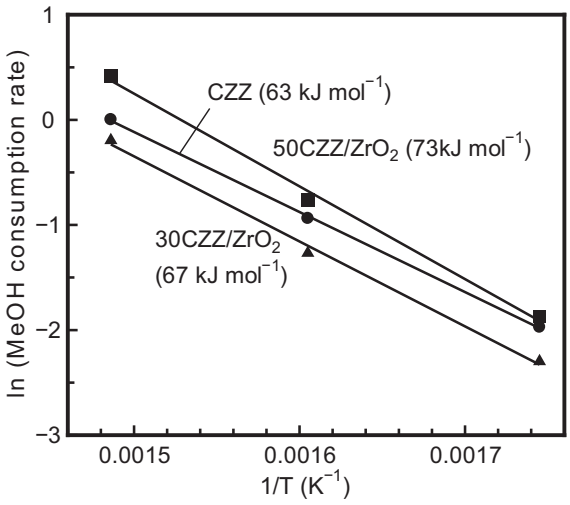

Fig. 12. Arrhenius plots of methanol consumption rate at the conversion of 50%. Circle symbols, CZZ; square, 50CZZ/ZrO_2; triangle, 30CZZ/ZrO_2.

is considered that CO by-production by RWGS is rather promoted along with the sintering of Cu particles. Ritzkopf et al. discussed that presence of Cu^+ species suppresses CO by-production [27], but the XPS for Cu/ZnO/ZrO_2 with the Cu crystallite size of 14 nm shows that the surface of the Cu particles is metallic [7].

3.6. Apparent activation energy of the Cu catalysts

In order to obtain the apparent activation energy of the catalyst, the activities at 350 and 300 °C were measured after the reaction at 400 °C (see Fig. 5). Since the activities at 350 and 300 °C are fairly stable, the surface properties at these temperatures are similar to that just after the reaction at 400 °C for 5 h. Hence, the activation energy obtained will not be affected by the deactivation during the reaction at 350 or 300 °C significantly. Another set of the reaction was carried out under W/F of 0.0091 g h dm^{-3}. The values of $1/(1-C)$ relates to W/F also in the reactions at 350 and 300 °C (Fig. 11). The values at 400 °C are obtained from the final conversion at 400 °C (5 h-on-stream, see Fig. 5). On the basis of the data, the methanol consumption rates at the conversion of 50% are estimated and the apparent activation energies (E_a) are obtained from the Arrhenius plots (Fig. 12). The E_a for CZZ is 63 kJ mol^{-1} and discernibly lower than those for 50CZZ/ZrO_2 (73 kJ mol^{-1}) and 30CZZ/ZrO_2 (67 kJ mol^{-1}). The value of E_a reported for Cu/ZnO/Al_2O_3 is 76–105 kJ mol^{-1} [22,23,28] and that for Cu/ZrO_2/CeO_2 is 61–109 kJ mol^{-1} [29]. The activation energies for 50 and 30CZZ/ZrO_2 are fairly close to that of CZZ. This suggests that there is no decisive difference in the nature of the active sites on these catalysts.

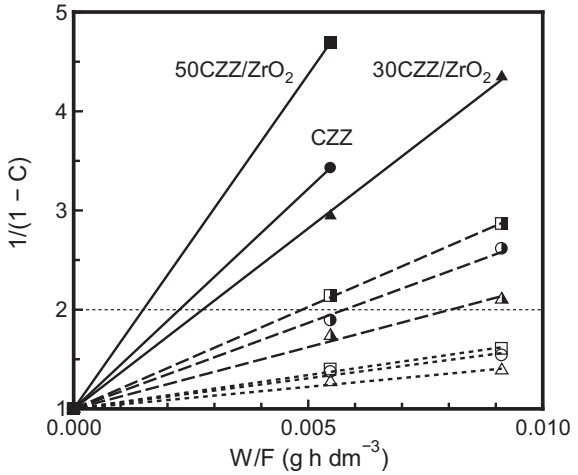

Fig. 11. Plots of $1/(1-C)$ vs. W/F on methanol conversions (C) for Cu catalysts at different reaction temperatures. Solid lines, 400 °C; broken lines, 350 °C; dotted lines, 300 °C; circle symbols, CZZ; square, 50CZZ/ZrO_2; triangle, 30CZZ/ZrO_2.

4. Conclusions

The coprecipitate of Cu/ZnO/ZrO_2 can be deposited on the surface of a zirconia support. The coprecipitated particles do not cover the support surface completely. While there is no significant difference in the crystallite sizes of the coprecipitated particles after the calcination at 500 °C between the catalysts with and without the support, the Cu crystallite size for the supported catalyst is discernibly smaller than that without the support after the high temperature methanol steam reforming at 400 or 500 °C. Thus, the sintering of Cu particles during the reaction can be suppressed by virtue of the presence of the support. The Cu surface amount decreases with a decrease in the Cu content of the supported catalysts, but the Cu dispersion for the supported catalyst is significantly higher than that for unsupported one. Although the Cu content of 50CZZ/ZrO_2 is a half of that in the catalyst without the support (CZZ), the catalytic activity after the reaction at 400 or 500 °C is higher than that of the latter. This is because of the high Cu surface activity (TOF) of the supported catalyst probably due to the small Cu particle size as a result of the suppression of sintering. The apparent activation energies for the supported and unsupported catalysts are 63–73 kJ mol^{-1}. The CO selectivity increases with an increase in the mean Cu crystallite size, suggesting that the sintering of Cu particles enhances CO by-production. In conclusion, the coprecipitation of Cu/ZnO/ZrO_2 on the zirconia support results in higher activity, durability, and selectivity in methanol steam reforming with a smaller Cu content by virtue of prevention of Cu sintering.

References

[1] G.C. Chinchen, P.J. Denny, J.R. Jennings, M.S. Spencer, K.C. Waugh, Appl. Catal. 36 (1988) 1–65.

[2] S. Sá, H. Silva, L. Brandão, J.M. Sousa, A. Mendens, Appl. Catal. B 99 (2010) 43–57.
[3] D.R. Palo, R.A. Dagle, J.D. Holladay, Chem. Rev. 107 (2007) 3992–4021.
[4] A. Qi, B. Peppley, K. Karan, Fuel Process. Technol. 88 (2007) 3–22.
[5] M.S. Wilson, Int. J. Hydrogen Energy 34 (2009) 2955–2964.
[6] Y. Matsumura, H. Ishibe, Appl. Catal. B 91 (2009) 524–532.
[7] Y. Matsumura, H. Ishibe, J. Mol. Catal. 345 (2011) 44–53.
[8] J.P. Breen, J.R.H. Ross, Catal. Today 51 (1999) 521–533.
[9] J. Agrell, H. Birgersson, M. Boutonnet, I. Melián-Cabrera, R.M. Navarro, J.L.G. Fierro, J. Catal. 219 (2003) 389–403.
[10] C.-L. Li, Y.-C. Lin, Catal. Lett. 140 (2010) 69–76.
[11] S.D. Jones, E. Hagelin-Weaver, Appl. Catal. B 90 (2009) 195–204.
[12] W.-J. Shen, Y. Matsumura, J. Mol. Catal. A 153 (2000) 165–168.
[13] F. Moreau, G.C. Bond, A.O. Taylor, J. Catal. 231 (2005) 105–114.
[14] Y. Matsumura, H. Ishibe, J. Power Sources 209 (2012) 72–80.
[15] C. Hammond, The Basics of Crystallography and Diffraction, Oxford University Press, New York, 1997, pp. 145–148.
[16] ISO 18118, 2004.
[17] J.W. Evans, M.S. Wainright, A.J. Bridgewater, D.J. Young, Appl. Catal. 7 (1983) 75–83.
[18] ICDD Files, 821253, 410254, 211486, 170923, 371484, and 40836.
[19] P.H. Matter, D.J. Braden, U.S. Ozkan, J. Catal. 223 (2004) 340–351.
[20] Y. Murase, F. Nishikawa, K. Daimon, E. Kato, Int. J. High Technol. Ceram. 4 (1988) 86.
[21] C.D. Wagner, in: D. Briggs, M.P. Seah (Eds.), Practical Surface Analysis, second ed., Auger and X-ray Photoelectron Spectroscopy, vol. 1, John Wiley & Sons, Inc., New York, 1990, pp. 595–634.
[22] J. Agrell, H. Birgersson, M. Boutonnet, J. Power Sources 106 (2002) 249–257.
[23] H. Purnama, T. Ressler, R.E. Jentoft, H. Soerijanto, R. Schlögl, R. Schomäcker, Appl. Catal. A 259 (2004) 83–94.
[24] B.A. Peppley, J.C. Amphelett, L.M. Kearns, R.F. Mann, Appl. Catal. A 179 (1999) 21–29.
[25] B.L. Kniep, F. Girgsdies, T. Ressler, J. Catal. 236 (2005) 34–44.
[26] F. Arena, K. Barbera, G. Italiano, G. Bonura, L. Spadaro, F. Frusteri, J. Catal. 249 (2007) 185–194.
[27] I. Ritzkopf, S. Vukojević, C. Weidenthaler, J.-D. Grunwaldt, F. Schüth, Appl. Catal. A 302 (2006) 215–223.
[28] J.K. Lee, J.B. Ko, D.H. Kim, Appl. Catal. A 278 (2004) 25–35.
[29] A. Mastalir, B. Frank, A. Szizybalski, H. Soerijanto, A. Deshpande, M. Niederberger, R. Schomäcker, R. Schlögl, T. Ressler, J. Catal. 230 (2005) 464–475.